

Energy distributions of charged particles from three-body decay

E. Garrido ^{a,*}, D.V. Fedorov ^b, H.O.U. Fynbo ^b, A.S. Jensen ^b

^a *Instituto de Estructura de la Materia, CSIC, Serrano 123, E-28006 Madrid, Spain*

^b *Department of Physics and Astronomy, University of Aarhus, DK-8000 Aarhus C, Denmark*

Received 20 February 2006; received in revised form 24 October 2006; accepted 8 November 2006

Available online 27 November 2006

Abstract

We compute the energy distributions of charged particles and neutrons emerging from the three-body decay of the 2^+ -resonances of ${}^6\text{Be}$ and ${}^6\text{Li}$ with isospin 1. These states are isobaric analogue states to the 2^+ -resonance in ${}^6\text{He}$. We use hyperspherical adiabatic expansion combined with the complex scaling method. We first investigate the adiabatic potentials and the related eigenfunctions where each has its characteristic contribution to different energy distributions. The microscopic origin of the related decay mechanisms is exhibited. The Coulomb interaction in general broadens the distributions due to long-range couplings. The method is rather efficient in the present cases. Numerically stable distributions are found at intermediate hyperradii where the basis size is sufficient to describe the asymptotic behavior. Different decay mechanisms contribute with sequential α -emission as dominating but also with substantial fractions of direct decay. Computations are consistent with available experiments.

© 2006 Elsevier B.V. All rights reserved.

PACS: 21.45.+v; 31.15.Ja; 25.70.Ef

1. Introduction

Resonances decaying into three particles can be viewed as a direct generalization of α -particle emission. Three observables characterize these processes, i.e. total energy, partial decay width and energy distributions of the three particles appearing in the final state. The resonance energy is in general determined by many particles interacting in a possibly complicated structure which

* Corresponding author.

E-mail address: e.garrido@iem.cfmac.csic.es (E. Garrido).

can differ very much from a three-body state formed by the three particles in the final state. The partial decay width is essentially determined by the effective barrier appearing at intermediate distances in the three-body fragmentation of the final state particles. The decay mechanisms are closely related to the structures of the three-body resonances, and in particular to changes from small to large distances. These properties were discussed in two preceding papers [1,2].

The energy distributions of three short-range interacting particles in the final state were discussed in a subsequent paper [3]. These observables reflect the large-distance properties of the resonance wave function. Computations are numerically demanding because the resonance conditions imply exponentially increasing wave functions. This is circumvented by the complex scaling method where the coordinates are “rotated” by multiplication with a complex phase factor [4]. The large-distance asymptotic behavior then turns into exponentially decreasing functions, but now the energy distributions are determined by ratios of these exponentially small tails [3]. For short-range interactions the asymptotics is normally reached at moderate distances but narrow two-body resonances or attractive s -waves may significantly increase this convergence distance. Knowledge of these intermediate structures may be used to alleviate the numerical demands.

Another type of problem arises when more than one of the three particles is charged and the long-range Coulomb interaction has to be treated. Most of the experimental activities deal with such systems [5,6,8–19]. Energy distributions are measured with high accuracy in kinematically complete experiments. The purpose of the present paper is therefore to extend the theoretical descriptions to obtain reliable results with both short and long-range interactions. We shall use the hyperspherical expansion method combined with complex scaling [20,21] and assume that formation and decay of the resonances are independent processes. This method was used in [4,22] to compute the energies and widths of the 2^+ -resonances in ${}^6\text{He}$ ($\alpha + n + n$), ${}^6\text{Li}$ ($\alpha + n + p$) and ${}^6\text{Be}$ ($\alpha + p + p$). We shall use these cases as illustrative examples of results for energy distributions of fragments after three-body decay. Resonance energies and widths are also considered in several other previous publications [23–27], however no energy distributions of fragments have been reported so far. Two-proton radioactivity for heavier systems has been considered in [28].

The R -matrix theory based on decomposition into two-body subsystems is shown in [26] to lack direct three-body decay to reproduce the correct widths. The most recent calculation in [27] illustrates the difficulties inherent in any hyperspherical harmonic expansion method. The general nature of these problems call for a comparison with the present method [4,22] which differs decisively by the use of the three Faddeev components in the wave function.

In [27] hyperradii up to 1000 fm is needed because two particles can be close while the third one is far away. An extrapolation procedure is then used to circumvent the problem. The need for these large hyperradii is a signal of the frequently occurring sequential decay mode. Large values of the maximum hyperspherical quantum number (hypermomentum) K_{\max} is necessary with the hyperharmonic expansion. Both problems can be handled with inclusion of Faddeev components and individual treatment of the different partial waves within each of these components. Also explicit inclusion of the asymptotic behavior for direct or sequential decay may be advantageous [3]. Then moderate hyperradii are sufficient and large K_{\max} only needed for a few specific partial waves.

Another feature is the underbinding obtained by use of only two-body interactions although they reproduce all (low-energy) two-body scattering data. In [27] this is handled by adding a three-body interaction behaving as ρ^{-3} for large hyperradii. This is the same large-distance behavior as resulting from the two-body interactions and therefore only reflecting a correction to these, either due to direct inaccuracy or due to lack of freedom in a limited basis. In this sense this

is not a three-body interaction constructed to account for effects beyond the two-body level, i.e. all three particles must participate and without Coulomb interaction only a short-range behavior seems to be acceptable. This idea was first formulated and introduced in [29]. An alternative correction used in [27] is scaling of the nucleon-core interaction by a few per cent. This obviously has the effect of reproducing the selected three-body properties but at the same time the measured two-body continuum data are no longer reproduced. This is an obvious problem in computations of three-body properties arising from sequential decay where one pair of particles remain close and therefore sensitive to the two-body interaction.

A third problem is related to the treatment of couplings due to the Coulomb interaction. Formally the hyperradial ρ^{-1} -dependence is the same for diagonal and non-diagonal terms. The couplings extent to very large distances which only can be handled with an ever increasing basis reflected in the need for very large values of K_{\max} . A compromise must be reached with convergence before the basis size becomes too large. This is possible with Faddeev components [3] but impossible, or at least very difficult, with only one component.

In the present paper we use the same method and the same interaction parameters [4,22] to compute resonance energies, widths and energy distributions. Previously also ground state properties were investigated. Computations of many observables are the only severe success criteria for the model, because limitations to a few data points can too easily be reproduced by smaller individual adjustments of various model parameters. The paper is organized as follows. After the introduction in Section 1, we briefly sketch in Section 2 the theoretical framework including the numerical information from previous computations of the 2^+ -resonances in ${}^6\text{He}$. In Sections 3 and 4 we discuss the angular potentials and the resonance wave functions obtained from realistic computations of the decay of the analogue 2^+ -resonances in ${}^6\text{Li}$ and ${}^6\text{Be}$. In Section 5 we discuss the computed energy distributions. Finally, Section 6 contains a brief summary and the conclusions.

2. Theoretical formulation

We first sketch the general theoretical framework which previously was demonstrated to work for short-range interactions [3]. Then we specify the details needed for the new cases with the Coulomb interaction.

2.1. Computational procedure

The three-body resonance wave function Ψ is calculated in coordinate space after complex scaling by a finite angle θ . In the adiabatic hyperspherical expansion the wave function is expanded in terms of a complete set of angular functions $\{\Phi_n(\rho, \Omega)\}$,

$$\Psi(\mathbf{x}, \mathbf{y}) = \sum_n f_n(\rho) \Phi_n(\rho, \Omega), \quad (1)$$

where (\mathbf{x}, \mathbf{y}) are the mass scaled Jacobi coordinates in one of the three possible sets and (ρ, Ω) are the hyperradius and the five hyperangles associated to \mathbf{x} and \mathbf{y} . The angular functions are expanded in terms of the hyperspherical harmonics and they are obtained as the eigenfunctions of the angular part of the Faddeev equations. The corresponding radial coefficients (radial functions) $f_n(\rho)$ are obtained from a coupled set of radial equations where the eigenvalues of the angular part enter as effective adiabatic potentials [20].

When the complex scaling angle is larger than the argument of a given resonance, the corresponding radial coefficients in the adiabatic expansion decrease exponentially as functions of the

hyperradius [4]. For short-range potentials the asymptotic pre-exponential factors are constants. The long-range Coulomb interaction modifies the pre-exponential factors but leaves intact the dominating exponential decay. The functions which asymptotically vanish exponentially can be easily found numerically by solving the radial equations with e.g. a simple box boundary condition at larger distances. In fact exponentially vanishing functions are insensitive to the precise formulation of the boundary condition, be it simply zero at some box length or matching to a decaying exponent. Thus the radial functions $f_n(\rho)$ can be calculated numerically at a given ρ with high precision even with approximate boundary conditions, e.g. box boundary, simply by moving the boundary to distances larger than the required ρ by several decay-lengths.

We now assume that when particles reach some large distance ρ_{\max} the Coulomb interaction further on can be neglected. In other words we cut off the Coulomb interaction at this distance. The analytically unknown Coulombic pre-exponential factors become constants after the cut-off and we effectively get the asymptotics for short-range potentials where the radial functions are (complex scaled) free radial waves.

Hyperspherical harmonics with free radial waves transform into themselves after Fourier transformation and the kinetic energy distribution of the fragments after decay of the resonance is therefore, except for a phase-space factor, obtained as the absolute square of the total wave function in coordinate space for the large value ρ_{\max} of the hyperradius, but where the five hyperangles are interpreted as in momentum space [3]. After integration over the four hyperangles describing the directions of the two Jacobi momenta, \mathbf{k}_x and \mathbf{k}_y , conjugate to \mathbf{x} and \mathbf{y} , the probability distribution as function of $k_y^2 \propto \cos^2 \alpha$, where α is the fifth momentum hyperangle, is given by

$$P(k_y^2) \propto P(\cos^2 \alpha) \propto \sin(2\alpha) \int d\Omega_x d\Omega_y |\Psi(\rho_{\max}, \alpha, \Omega_x, \Omega_y)|^2. \quad (2)$$

In the same way as y is proportional to $\cos \alpha$, k_y is also proportional to $\cos \alpha$, but in momentum space. Except for some mass factors k_y is the momentum of the third particle from the three-body center of mass. Therefore the kinetic energy of the third particle is proportional to k_y^2 (or to $\cos^2 \alpha$), and the energy distribution then is as given in Eq. (2). In particular, $\cos^2 \alpha$ gives the energy of the particle relative to its maximum possible energy in the decay process.

We shall check numerically that the energy distribution of fragments we calculate is insensitive to ρ_{\max} by calculating the distribution for different values of ρ_{\max} where we shall refer to ρ_{\max} simply as ρ .

This procedure has formally the shortcoming that the hyperradius in Eq. (2) in principle should be asymptotically large (since the detection takes place at large distance), and the larger values of ρ the larger basis size is required for the hyperspherical expansion. For short-range potentials the asymptotic limit is known to be the hyperspherical harmonics reflected in the corresponding hyperharmonic spectrum of the Hamiltonian without interaction. It was shown in previous reports [3] that the correct asymptotic limit is reached already at intermediate distances where the basis size is still manageable in the numerical calculations. An increase of ρ then requires a larger basis which then would reproduce the energy distribution found at the smaller distance with the smaller basis size. This optimum region of hyperradii is determined as the region where the observable is independent of ρ -variations; further increase of ρ is not productive. Clearly this is a satisfactory procedure for short-range interactions.

An extension to include the long-range Coulomb interaction is not obvious. The Coulomb interaction couples different adiabatic potentials to very large hyperradii by amounts similar to corresponding diagonal contributions. This is not a problem as long as the basis size is large

enough to describe the resulting variation in the radial wave functions. However, with couplings extending to infinity the required basis size would at some point become too large to be handled numerically. The problem to find numerically a compromise between the size of the basis and the maximum value of ρ is similar to that for short-range interactions where the solution was to stop at intermediate values of ρ and look for a stable region with energy distributions independent of ρ . This is a practical approach which only can be tested by numerical investigations. A similar method has been tried in atomic physics [30] where extrapolation to large distances in addition was employed.

This procedure was also applied to the nuclear 2^+ -resonance in ${}^6\text{He}$ where only short-range interactions enter [3]. We found that the resonance structure changed substantially from small to large distances. The α -neutron two-body $p_{3/2}$ -resonance dominates at small distance and the neutron–neutron s -wave at large distance. The implication for the energy distributions is that the maximum α -particle energy is preferred as correspondingly intermediate neutron energies. The next step is to include the Coulomb interaction and study the effects.

2.2. Details of the calculations

The 2^+ analogue states in ${}^6\text{Li}$ and ${}^6\text{Be}$ are, by definition, of the same structure as the 2^+ -resonance in ${}^6\text{He}$, which recently was investigated in details [3]. The large-distance behavior seen in the energy distributions should then reflect the influence of the Coulomb interaction. Thus we know the resonance structure, the decay mechanism and the energy distributions for this similar ${}^6\text{He}$ structure deviating from ${}^6\text{Li}$ and ${}^6\text{Be}$ only due to the absence of Coulomb interactions. These analogue states are then ideally suited for studying the influence of the Coulomb potential. The nuclear two-body potentials used in the calculations are specified in [31], and the three-body interactions are from [22].

The calculations have been performed including relative orbital angular momenta between the three possible pairs of particles up to $\ell = 11$, with a maximum value of the hypermomentum K equal to 20 for all the components except for those found to dominate the three-body structure. These large components are described by K_{max} -values individually adjusted to provide the necessary accuracy. They are specified in Table 1. For ${}^6\text{Be}$ and ${}^6\text{He}$ only nucleon–nucleon isospin equal to 1 is allowed or equivalently $\ell_x + s_x$ has to be even for components in the first Jacobi set. However, for ${}^6\text{Li}$ an isospin 0 neutron–proton admixture into the isobaric analogue state is allowed due to the isospin breaking Coulomb interaction. This interaction has been taken from [32].

The scaling angles used in the calculations are 0.10 rad for ${}^6\text{Li}$ and 0.15 rad for ${}^6\text{Be}$. They are chosen to exceed the corresponding angles for the resonances by a sufficient amount to provide unique bound state conditions at relatively small distances. The experimental energies and widths (E_R, Γ) for the analogue 2^+ resonances in ${}^6\text{Li}$ and ${}^6\text{Be}$ are (1.67, 0.54) MeV and (3.04, 1.16) MeV, respectively [33]. The energies computed with the two short-range interactions supplemented by the appropriate Coulomb potentials are (1.92, 0.87) MeV and (3.10, 1.89) MeV. The computed ${}^6\text{He}$ state is bound by 0.15 MeV less than the measured value. Thus attractive three-body interactions are necessary for fine tuning. If we choose a Gaussian shape with a range of 3 fm in hyperradius and then adjust the strength to reproduce the energy positions we get (1.64, 0.53) MeV for ${}^6\text{Li}$ and (3.02, 1.65) MeV for ${}^6\text{Be}$, respectively the same and about 50% too large compared to the experimental widths [22].

Table 1

Components included in the three-body calculations have $K_{\max} = 20$ except those specified here. The left part refers to the components in the first Jacobi set (x connecting the two nucleons), and the right part to the ones in the second and third Jacobi sets (x connecting the alpha-particle and one of the nucleons)

1st Jacobi set						2nd and 3rd Jacobi sets					
ℓ_x	ℓ_y	L	s_x	s_y	K_{\max}	ℓ_x	ℓ_y	L	s_x	s_y	K_{\max}
0	2	2	0	0	180	0	2	2	1/2	0	44
2	0	2	0	0	180	0	2	2	1/2	1	44
1	1	1	1	1	180	2	0	2	1/2	0	70
1	1	2	1	1	64	2	0	2	1/2	1	44
2	2	2	0	0	90	1	1	1	1/2	1	240
1	3	2	1	1	42	1	1	2	1/2	0	240
3	1	2	1	1	42	1	1	2	1/2	1	44
2	4	2	0	0	54	2	2	1	1/2	1	32
4	2	2	0	0	54	2	2	2	1/2	0	50
4	4	2	0	0	68	2	2	2	1/2	1	42
						1	3	2	1/2	0	42
						1	3	2	1/2	1	42

3. Angular eigenvalues and eigenfunctions

The details of the calculated structure of the 2^+ three-body wave functions are given in this and the following section. As shown in Eq. (1), the adiabatic expansion separates the radial and the angular coordinates. To obtain an accurate three-body wave function the crucial quantities are then the adiabatic potentials and their related angular wave functions, i.e. the eigenvalues and eigenfunctions of the angular part of the Faddeev equations.

3.1. Adiabatic potentials

The numerical solutions first provide the angular eigenvalues λ_n as functions of the hyper-radius ρ . The adiabatic potentials $V_{\text{eff}}(\rho)$ are then essentially obtained by dividing with ρ^2 and adding the centrifugal terms proportional to ρ^{-2} [20]:

$$V_{\text{eff}}(\rho) = \frac{\hbar^2 \lambda_n(\rho) + 15/4}{2m \rho^2}. \quad (3)$$

The results are shown in Figs. 1 and 2 for the 2^+ -resonances in ${}^6\text{Be}$ and ${}^6\text{Li}$, respectively. The usual features from only short-range interactions are clearly visible for the potentials, i.e. an attractive region at small distance, barriers for the lowest potentials at intermediate distances, and the decrease at large distance towards zero. Many levels are close-lying or crossing each other at relatively small distances. For ${}^6\text{Li}$ the lowest potential corresponds at large distances essentially to a deuteron in the ground state and a non-interacting α -particle in a relative d -wave. This configuration has symmetric neutron–proton relative wave function.

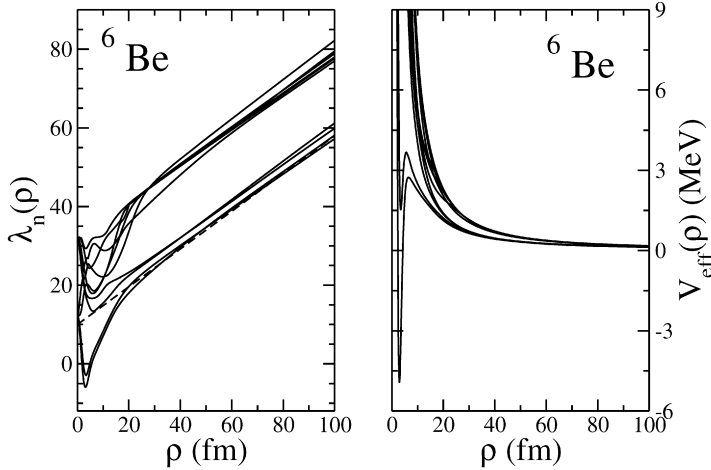


Fig. 1. Real parts of the lowest 10 angular eigenvalues (left) and their corresponding adiabatic potentials (right) as functions of ρ for the 2^+ -resonance in ${}^6\text{Be}$. The scaling angle is $\theta = 0.15$. The dashed line is the estimated behavior at large distances for the lowest angular eigenvalue according to Eq. (6). They are numbered from below at maximum ρ .

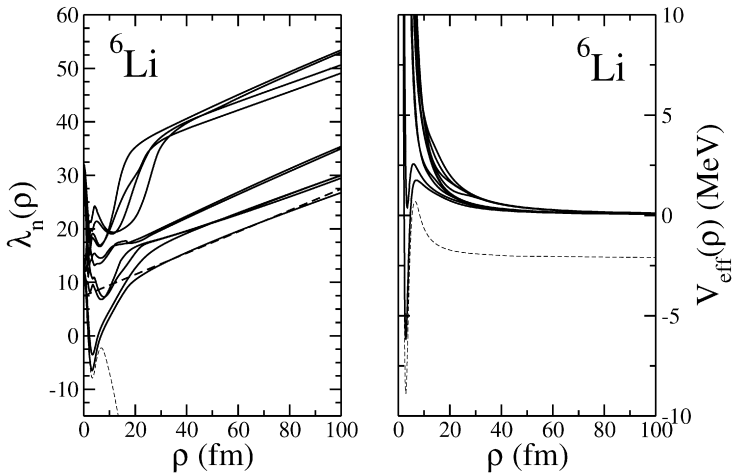


Fig. 2. The same as Fig. 1 for the 2^+ -resonance in ${}^6\text{Li}$. The scaling angle is 0.10 . The states are numbered to correspond to Fig. 1, i.e. the lowest bound deuteron state can naturally be labeled by 0. The thick dashed line in the left part is the estimate from Eq. (6).

The detailed behavior is exhibited by the large-distance linear dependence of the angular eigenvalues. This simply reflects ρ^2 multiplied on the ρ^{-1} form of the Coulomb potential V_C given by

$$V_C = \sum_{j < k} \frac{Z_j Z_k e^2}{r_{jk}} = \sum_{j < k} \mu_i \frac{Z_j Z_k e^2}{\rho \sin \alpha_i}, \quad \mu_i \equiv \sqrt{\frac{m_j m_k}{(m_j + m_k)m}}, \quad (4)$$

where eZ_j and m_j are the charge and mass of particle j , and $|\mathbf{x}_i| = \rho \sin \alpha_i = \mu_i r_{jk}$ is the mass scaled distance between particles j and k . The sizes of the slopes of the angular eigenvalues in Figs. 1 and 2 can then be estimated by use of perturbation theory and the free wave functions,

i.e. by the expectation value of the Coulomb operator for the hyperspherical harmonics. These kinetic energy eigenfunctions are characterized by a hyperspherical quantum number K and a set of angular momentum quantum numbers (ℓ_x, ℓ_y) . Each term in Eq. (4) is expressed in one set of Jacobi coordinates, and the slopes of λ_n are therefore easily estimated by

$$\begin{aligned} \frac{\partial \lambda}{\partial \rho} &= \frac{2m}{\hbar^2} \mu_i Z_j Z_k e^2 \frac{\int_0^{\pi/2} \sin^{2\ell_x+1} \alpha \cos^{2\ell_y+2} \alpha d\alpha}{\int_0^{\pi/2} \sin^{2\ell_x+2} \alpha \cos^{2\ell_y+2} \alpha d\alpha} \\ &= \frac{2m}{\hbar^2} \mu_i Z_j Z_k e^2 \frac{2}{\pi} \frac{(2\ell_x)!!(2\ell_x + 2\ell_y + 4)!!}{(2\ell_x + 1)!!(2\ell_x + 2\ell_y + 3)!!} \\ &= \frac{2m}{\hbar^2} \mu_i Z_j Z_k e^2 \frac{2^{4\ell_x+2\ell_y+5}}{\pi} \frac{(\ell_x!(\ell_x + \ell_y + 2)!)^2}{(2\ell_x + 1)!(2\ell_x + 2\ell_y + 4)!}, \end{aligned} \quad (5)$$

where we assumed zero nodes in the Jacobi polynomial (then a constant) related to the α -coordinate. We use the notation !! for the product of every other integer number down to 1 or 2. The (ℓ_x, ℓ_y) components transform into different linear combinations of angular momenta in another set of Jacobi coordinates. The $(\ell_x, \ell_y) = (0, 0)$ wave functions transform only into itself and we get in this case [34]

$$\frac{\partial \lambda}{\partial \rho} = \frac{2m}{\hbar^2} \frac{16}{3\pi} \sum_{j < k} \mu_i Z_j Z_k e^2, \quad (6)$$

which is about 0.50 fm^{-1} for ${}^6\text{Be}$ and 0.21 fm^{-1} for ${}^6\text{Li}$ roughly in agreement with Figs. 1 and 2.

The angular momentum dependence can only be estimated easily for each term. However, for ${}^6\text{Li}$ there is only one such term, which also is the largest of the (two identical) ${}^6\text{Be}$ -terms, arising from the two α -proton interactions. From Stirling's formula we immediately derive from Eq. (5) that one of the Coulomb terms changes from the value in Eq. (6) to

$$\frac{\partial \lambda}{\partial \rho} \approx \frac{2m}{\hbar^2} \mu_i Z_j Z_k e^2 2\sqrt{\frac{\ell_y}{\pi}} \quad (7)$$

in the limit when $\ell_y \gg 1$ and ℓ_x remains zero. This term increases for ${}^6\text{Li}$ from the value 0.21 fm^{-1} for $(\ell_x, \ell_y) = (0, 0)$ as $0.140\sqrt{\ell_y} \text{ fm}^{-1}$ for $\ell_x = 0$ and $\ell_y \gg 1$. For $\ell_x \gg 1$, and independent of ℓ_y , the behavior derived from Eq. (5) is

$$\frac{\partial \lambda}{\partial \rho} \approx \frac{2m}{\hbar^2} \mu_i Z_j Z_k e^2 \sqrt{1 + \ell_y/\ell_x}, \quad (8)$$

which provides the limits of 0.124 fm^{-1} for $\ell_y = 0$ and $\ell_x \gg 1$, and 0.175 fm^{-1} for $\ell_x = \ell_y \gg 1$, and $0.124\sqrt{\ell_y/\ell_x} \text{ fm}^{-1}$ for $\ell_y \gg \ell_x \gg 1$. The term with large ℓ_y increases as $\sqrt{\ell_y}$ for $\ell_x = 0$, and as $\sqrt{\ell_y/\ell_x}$ for $\ell_x > 0$.

The relevant comparison to the numerical values is most likely for roughly equal values of ℓ_x and ℓ_y and both sum and difference less than the total angular momentum of the resonance. Then an estimate of a weighted average would be the value for $(\ell_x, \ell_y) = (0, 0)$ since the other limit of very large and equal angular momenta only is 17% smaller. The strong variation in the slopes occurs in the rather unlikely cases when ℓ_y becomes much larger than ℓ_x . However, the Coulomb interaction dominates at large distance over centrifugal barrier terms. The dependence on angular momentum quantum numbers can then be expected to decrease with ρ implying that all slopes should be of the same magnitude. This is confirmed by the estimates shown by the

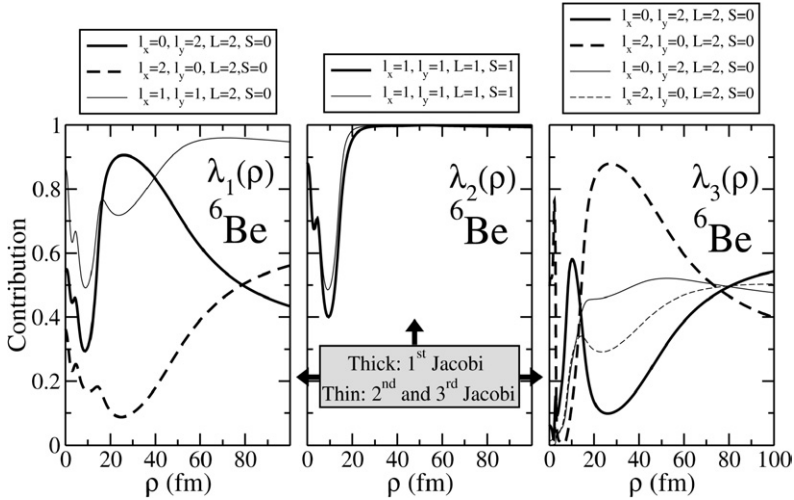


Fig. 3. The fraction of the dominating components in the angular eigenfunction (the sum, normalized to unity, of the three Faddeev components, rotated into the given Jacobi set of coordinates) for the three lowest adiabatic potentials as function of ρ for ${}^6\text{Be}$ (2^+), see Fig. 1. The quantum numbers are as given in Table 1. Thick lines: Jacobi coordinates where x refers to the two-proton system and y to its center of mass motion relative to the α -particle. Thin lines: Jacobi coordinates where x refers to the proton- α system and y to its center of mass motion relative to the other proton.

dashed lines in the left parts of Figs. 1 and 2. It is remarkable that the asymptotic slope only is attained by bending the angular eigenvalues around 20–30 fm. This bending is therefore not an artifact of the numerical procedure. This is confirmed by increasing both basis size and the number of partial waves in the computation.

The imaginary parts of the angular eigenvalues are not shown in Figs. 1 and 2 to avoid cluttering the figures. They are much smaller than the real parts, increasing linearly with a relatively small slope [4].

3.2. Adiabatic wave functions

The angular wave functions related to the adiabatic potentials are functions of ρ , see Eq. (1). As a consequence, the contributions from different partial wave components can also vary with ρ . Furthermore, the partial wave expansion is different in the three different sets of Jacobi coordinates. In Fig. 3 we show the details of the variation of the weights of the most relevant angular momentum components for the three first angular eigenvalues for the 2^+ -resonance in ${}^6\text{Be}$. The second and third Jacobi sets are identical (x coordinate between the core and one of the protons). The numbering of these λ 's is made from bottom to top at the maximum value of ρ in Fig. 1. Therefore, the lowest three λ 's are the expected three most decisive ones at large values of ρ , i.e. in the region of ρ -values where the energy distributions after decay of the resonance are determined. In the figure only the most contributing partial wave components at large ρ are shown.

The first eigenfunction (left part of Fig. 3) is at small ρ essentially an s -wave in the relative motion of the two protons and a d -wave in their common motion relative to the α -particle (the solid thick curve dominates). This implies that the two proton spins couple to zero to achieve an antisymmetric wave function. This contribution is maximum (more than

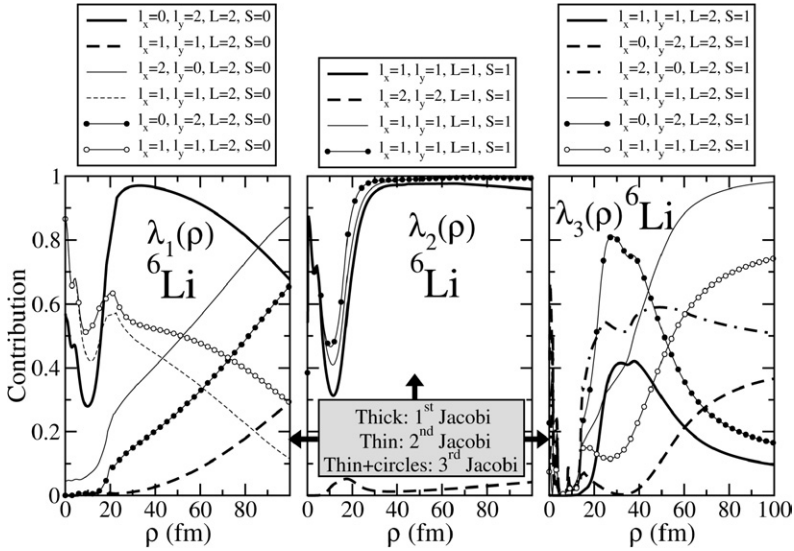


Fig. 4. The same as in Fig. 3 for the corresponding 2^+ -resonance in ${}^6\text{Li}$, except that we omitted the almost decoupled lowest eigenfunction of deuteron- α character. In the second Jacobi set (thin lines) the x refers to the proton- α system and y to its center of mass motion relative to the neutron. In the third Jacobi set (thin + circle lines) the x refers to the neutron- α system and y to its center of mass motion relative to the proton.

90%) at distances between 20 and 40 fm, starting afterwards a quick reduction to about 40% at $\rho = 100$ fm. At this distance the main contribution (almost the remaining 60%) is given by the component where d - and s -waves are interchanged (thick dashed curve). This structure is equivalent to equal amounts of the different α -proton p -waves consistent with the Pauli principle and parity and angular momentum conservation. The α -proton motion (second and third Jacobi system) is dominated by the p -wave contributions, specially for large ρ (thin solid line).

The second eigenfunction in Fig. 3 (central panel) has already at relatively small distances changed to about 100% proton–proton and α -proton p -waves which correspond to partial wave components with total spin $S = 1$. The third eigenfunction (right part) is dominated at intermediate distances by a d -wave proton–proton relative motion (thick solid line), but for large values of ρ its contribution reduces to 40%, while more than 50% is given by the relative proton–proton s -wave. For this eigenfunction the α -proton motion is dominated by relative s - and d -waves at large distances (thin solid and thin dashed lines) although the contribution of these components almost vanishes at very small values of ρ .

The angular wave functions for the corresponding 2^+ -resonance in ${}^6\text{Li}$ are shown in Fig. 4. Eigenfunction number 1 (left panel) is, as in the ${}^6\text{Be}$ case, for ρ -values around 20–100 fm clearly dominated by a relative s -wave between the two nucleons (solid thick line). However, when ρ increases this component decreases less than for ${}^6\text{Be}$, still being around 70% at $\rho = 100$ fm. The remaining 30% is mostly found in a relative p -wave between the two nucleons (dashed thick line) with total spin zero, i.e. with isospin zero. This combination of quantum numbers is, due to parity, strictly forbidden in the description of the deuteron wave function. At large ρ we also observe a significant contribution of a relative d -wave between proton and α (solid thin line) and an s -wave between the neutron and the α (solid thin line with black circles). This differs

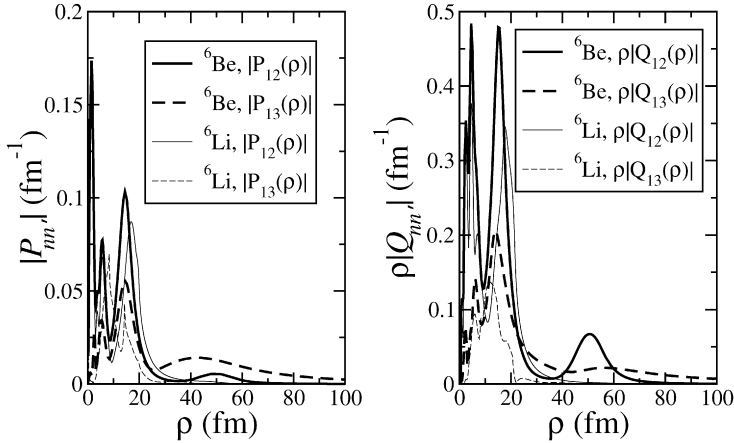


Fig. 5. The absolute values of the coupling potentials between the three lowest adiabatic levels for the 2^+ -resonance in ${}^6\text{Be}$ (thick curves $\theta = 0.15$ rad) as functions of ρ , and the corresponding isobaric analogue states in ${}^6\text{Li}$ (thin curves $\theta = 0.10$ rad).

from the first eigenfunction in ${}^6\text{Be}$, where a proton–proton relative p -wave was dominating at large distances.

The structure of eigenfunction number 2 (central panel) is very similar to the second in ${}^6\text{Be}$, where the relative neutron–proton, α -neutron, and α -proton p -waves clearly dominate for ρ values above 20 fm. We can see that in this case the weight of the p -wave neutron–proton contribution (solid thick curve) slightly decreases at large ρ , and the remaining contribution, small in any case, is given by a relative d -wave between neutron and proton with $S = 1$, and therefore also with neutron–proton isospin equal to 0.

The contributions from the zero isospin components in the neutron–proton system are specially significant in eigenfunction number 3 (right panel in Fig. 4). While an isospin 1 component with a p -wave neutron–proton motion (solid thick line) contributes around 10% at large distances, the isospin 0 components (thick dashed and thick dot-dashed curves) contribute all together with the remaining 90%.

4. Radial resonance wave functions

The diagonal potentials in the radial equations must be supplemented by the coupling terms. Their sizes and general behavior as function of ρ determine the total radial wave function, in particular at large ρ where the observable energy distributions are measured. In Fig. 5 we show the non-diagonal potentials involving the lowest level in ${}^6\text{Be}$ and its isobaric analogue in ${}^6\text{Li}$, and the two following ones for the 2^+ -resonance in ${}^6\text{Be}$ (thick lines) and ${}^6\text{Li}$ (thin lines). To show the first (P) and second (Q) order coupling potentials in the same units (fm^{-1}) we multiply Q by ρ . (The energy unit is restored in the coupling potentials by including the omitted factors, i.e. $\hbar^2 Q/(2m)$, $\hbar^2 P/(2m)\partial/\partial\rho$ [20].)

In both cases, ${}^6\text{Be}$ and ${}^6\text{Li}$, the behavior of the coupling potentials is similar. The strong variations at relatively small ρ are due to the rapidly changing structure of the angular eigenfunctions near the crossings between the λ -eigenvalues (see Figs. 1 and 2). The bump in the coupling potentials at around 50 fm is due to avoided crossing of the corresponding angular eigenvalues. The couplings are fortunately rather small at larger distances, although for intermediate distances

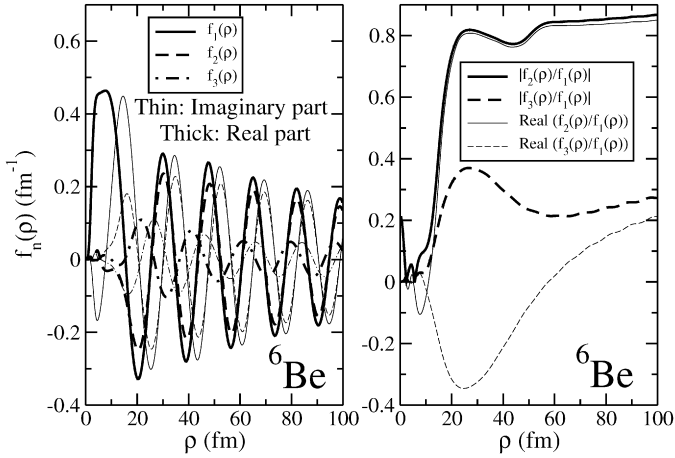


Fig. 6. Left: radial wave functions corresponding to the three first adiabatic potentials for the 2^+ -resonance in ${}^6\text{Be}$. The real and imaginary parts are shown by the thick and thin curves, respectively. Right: absolute values (thick curves) and the real parts (thin curves) of the ratios between the radial wave functions. The probability distribution has for each ρ been normalized to 1 as function of α .

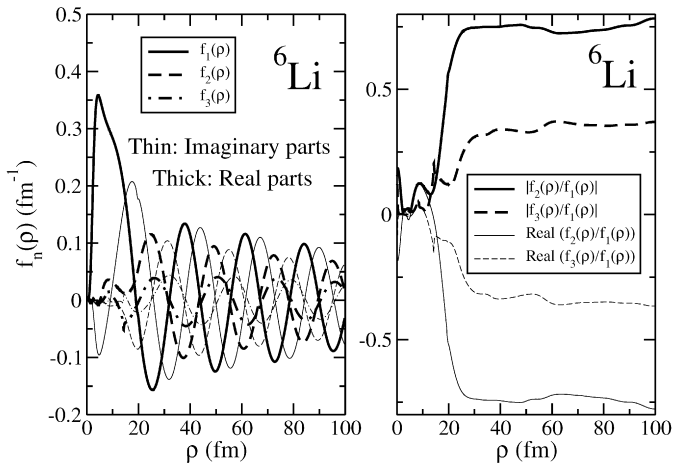


Fig. 7. The same as Fig. 6 for the corresponding 2^+ -resonance in ${}^6\text{Li}$.

the couplings in the ${}^6\text{Be}$ case are clearly larger than the ones for ${}^6\text{Li}$. This behavior is reassuring for the numerical computations because the radial wave functions can then be expected to be stable for distances larger than about 50 fm.

The solution to the coupled set of radial equations provides the radial resonance wave functions as function of ρ . The radial wave functions associated to the first three adiabatic potentials for the isobaric analogue 2^+ -resonances in ${}^6\text{Be}$ and ${}^6\text{Li}$ are shown in the left parts of Figs. 6 and 7, respectively. Under resonance conditions the amplitudes fall off exponentially with ρ in the complex scaled coordinates. However, each component still oscillates sinusoidally around zero while the amplitudes simultaneously decrease. Each component then vanishes and their asymptotic ratios determine the relative weights of the different adiabatic terms in the observables. Once the

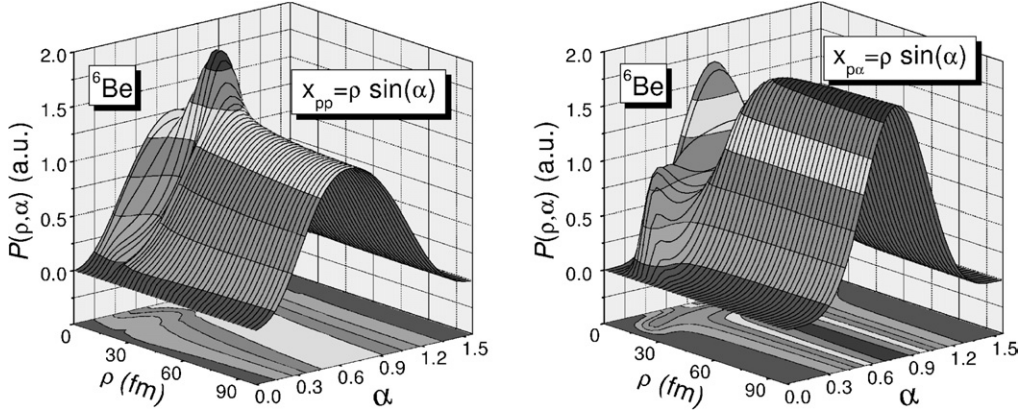


Fig. 8. The probability distribution for the 2^+ -resonance in ${}^6\text{Be}$ including the lowest 10 adiabatic potentials as function of the hyperradius ρ and hyperangle α related to the distance by $r_{ik} \propto \rho \sin \alpha$, i.e. the distance between either the one proton and core r_{pc} (right) or the two protons r_{pp} (left).

correct asymptotics is reached the different radial wave functions have the same analytical form, and the asymptotic ratios should then be constant. To reach this constant value is a numerically delicate task, especially if a long-range interaction (as the Coulomb potential) is present. This is because first the analytical form of this asymptotics is not known in the three-body case, and second because the radial wave functions could still be coupled at very large distances, requiring heavy numerical calculations in order to get accurate results for these large values of ρ .

To investigate this point we show in the right-hand side of Figs. 6 and 7 the absolute ratios (thick curves) involving the first three adiabatic terms entering the diagonal contributions to the energy distributions. In addition we show their corresponding real parts (thin curves), which enter in some of the non-diagonal contributions. Although they are not purely constant, in most of the cases they are relatively stable as functions of ρ for distances above 40–50 fm.

However, these variations are not in themselves a problem since the decreasing tendencies for some ratios are matched by increasing ratios of other radial wave functions, providing a rather stable total three-body wave function. This can be seen in Figs. 8 and 9, where we show the probability distributions (square of the three-body wave function integrated over the directions of the Jacobi coordinates x and y) for the isobaric analogue 2^+ -resonances in ${}^6\text{Be}$ and ${}^6\text{Li}$, respectively. These distributions are functions of the hyperradius ρ and the hyperangle α which are related to the distances between the pairs of particle by $r_{ik} \propto \rho \sin \alpha$, where r_{ij} refers to the distance between particles i and j .

In Fig. 8 it is seen that when ρ is above 50 fm the probability function stabilizes with a ridge at around $\alpha \approx \pi/4$ for which $x \approx y$. The same stabilization is found for ${}^6\text{Li}$, see Fig. 9, except perhaps the proton–neutron distribution (lower part). However, all these distributions arise from the same wave function expressed in different coordinate systems. The apparent variation can be related to inaccuracy in the coordinate transformations.

5. Energy distributions after three-body decay

As one can see from Eq. (2), the energy distributions are observables closely related to the probability distributions at asymptotically large distances. The only modification is due to the volume element corresponding to energy instead of momentum [3]. Therefore, from the prob-

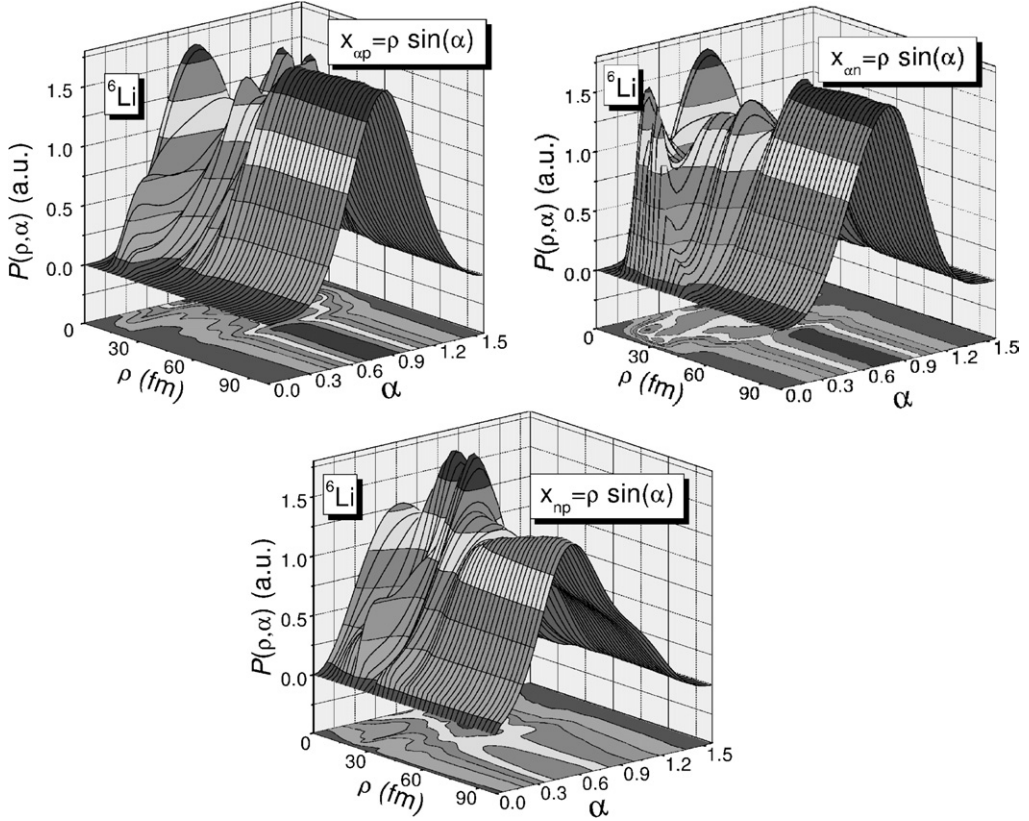


Fig. 9. The same as Fig. 8 for the corresponding 2^+ -resonance in ${}^6\text{Li}$. The distance $r_{ik} \propto \rho \sin \alpha$ refers to r_{cp} core–proton distance in the upper-left part, to the r_{cn} core–neutron distance in the upper-right part, and to the r_{pn} proton–neutron distance in the lower part.

ability distributions shown in Figs. 8 and 9 we obtain immediately the corresponding kinetic energy distributions for given ρ . For ${}^6\text{Be}$ we see in Fig. 10 the development from small to large distances as ρ increases. In the proton energy distribution (right), for small ρ two peaks are seen at small and large energies, that correspond to one proton populating a low-lying ${}^5\text{Li}$ ($\alpha + p$) resonance and the second proton taking most of the available energy. A wide central peak is also observed, that represent the contributions from structures where the α particle takes most of the energy. This structure changes into the asymptotic distribution of one broad peak at intermediate energy when ρ increases. This is the signature of a combination of direct decay [1] to get a broad peak and sequential decay by emission of the α -particle in opposite direction to the two protons.

The same signatures are found in the energy distribution of the α -particle, where the population for small ρ of a low-lying ${}^5\text{Li}$ -resonance produces a prominent central peak, while a structure where the α -particle takes most of the energy produces a shoulder at large energies. When ρ increases towards the relevant asymptotic distances the kinetic energy distributions have a clean tendency towards emission of high energy α -particles. However, the broad distribution indicates that a substantial part of the decay proceeds consistent with the direct decay mechanism where all distances between pairs of particles increase proportionally.

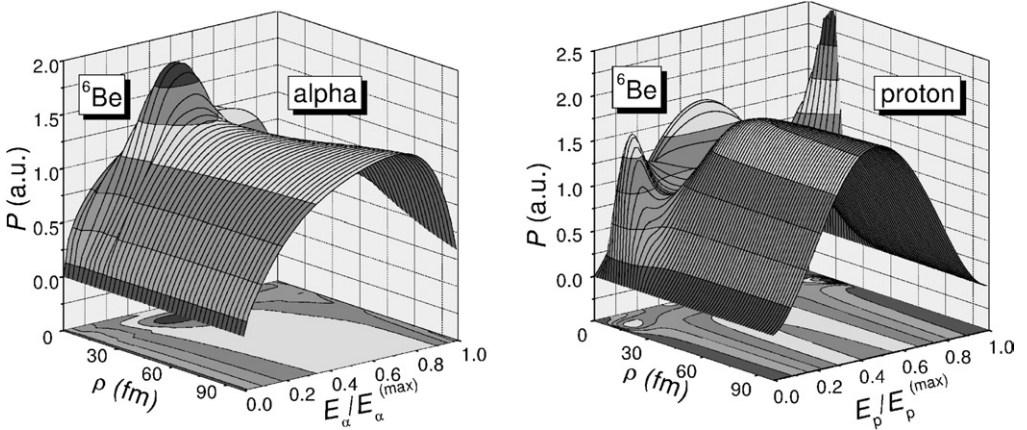


Fig. 10. Kinetic energy distributions of protons (right) and α -particles (left) after decay of the 2^+ -resonance in ${}^6\text{Be}$. The three-dimensional plots show the dependence on ρ with inclusion of 10 adiabatic wave functions as function of $\cos^2\alpha$, i.e. the kinetic energies $E_{\alpha,p}$ are in units of their maximum values $E_{\alpha,p}^{(\max)}$ given by $(m_\alpha + m_p)/(m_\alpha + 2m_p)E_R$ and $2m_p/(m_\alpha + 2m_p)E_R$ for the proton and the α -particle, respectively, where E_R is the energy of the decaying resonance.

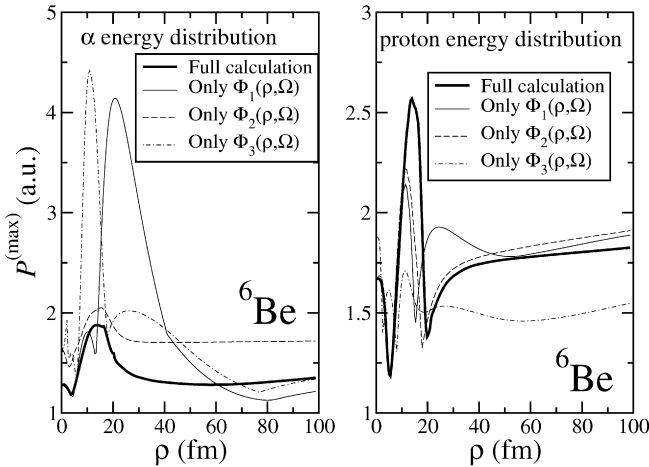


Fig. 11. Projections of kinetic energy distributions for ${}^6\text{Be}$ -decay. Thick curves: Projection of the α (left panel) and proton (right panel) kinetic energy distributions (Fig. 10) on the $E_{\alpha,p}/E_{\alpha,p}^{(\max)} = 1$ plane. They are then the profile originating from the maximum values of the energy distribution for each value of ρ . The thin curves are the same profile but when respectively only the first adiabatic term (solid), only the second adiabatic term (dashed), or only the third adiabatic term (dot-dashed) is included in the calculation.

As seen in Fig. 10, for ρ values above 40–50 fm the surface of the kinetic energy distributions is rather smooth and stable, indicating numerical convergence. However, this stability is the result of all the contributions coming from the 10 adiabatic potentials included in the calculations, although the individual contributions for some of them may be less stable. This is illustrated in Fig. 11, where the thick lines show the profile of the energy distributions in Fig. 10, i.e., the projection of the kinetic energy distributions on the plane defined by $E_{\alpha,p}/E_{\alpha,p}^{(\max)} = 1$. The first and third adiabatic potentials in Fig. 11 are not quite stable as function of ρ (specially

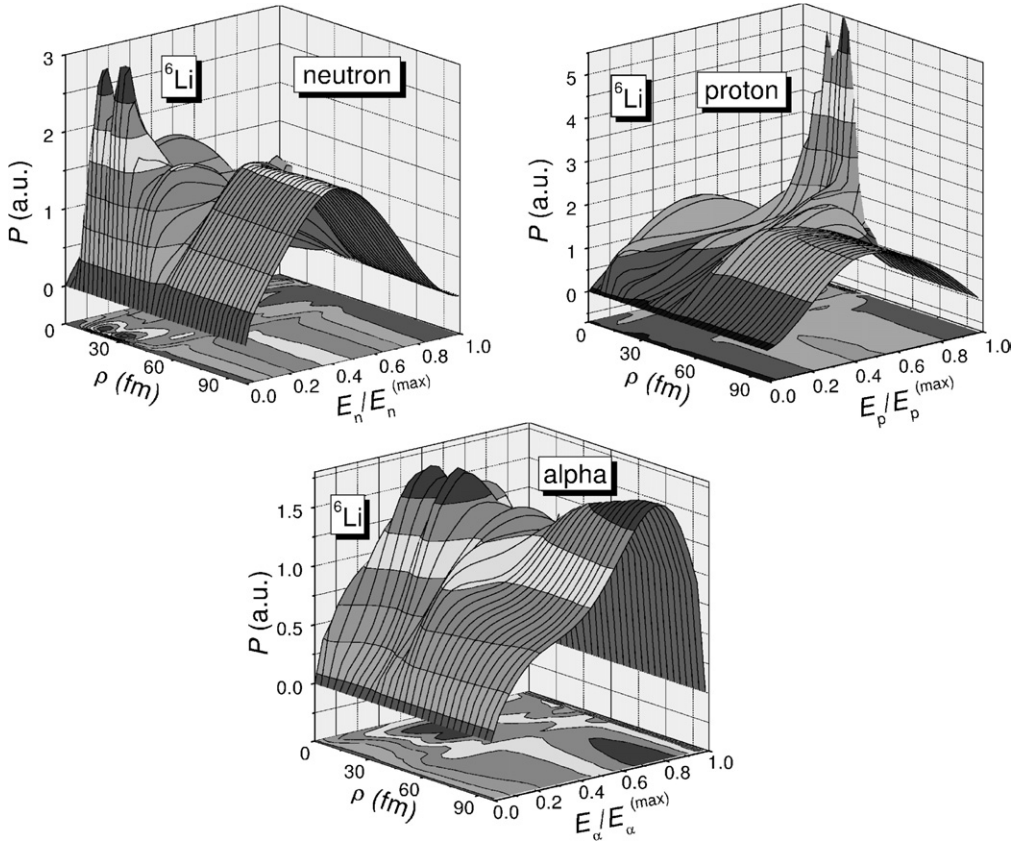


Fig. 12. Kinetic energy distributions of protons (upper-right panel), neutrons (upper-left panel), and α -particles (lower panel) after decay of the 2^+ -resonance in ${}^6\text{Li}$ corresponding to that of Fig. 10. The three-dimensional plot show the dependence on ρ with inclusion of 10 adiabatic wave functions. The maximum energies $E_{n,p,\alpha}^{(\max)}$ are $(m_\alpha + m_p)/(m_\alpha + m_n + m_p)E_R$, $(m_\alpha + m_n)/(m_\alpha + m_n + m_p)E_R$ and $(m_n + m_p)/(m_\alpha + m_n + m_p)E_R$ for the neutron, the proton, and the α -particle, respectively, where E_R is the energy of the decaying resonance.

for the α -particle energy distribution shown in the left side). Nevertheless these variations are compensated by the contribution from higher potentials and the total distribution (thick curve) becomes stable. Also the important contribution from the very stable second adiabatic potential (as seen from the right side of Fig. 6, where $|f_2/f_1| \approx 0.9$) contributes to stabilize the total distribution.

The kinetic energy distributions of the particles arising from the decay of the corresponding 2^+ -resonance in ${}^6\text{Li}$ are shown in Fig. 12. The distributions as well as their variations with ρ are mutually very different and in addition different from the distributions appearing from decay of ${}^6\text{Be}$. For small values of ρ the three-body structure is consistent with a mixture of two configurations, one where the low-lying p -resonance in ${}^5\text{He}$ is populated (peak at small energies for the neutron distribution, for large energies for the proton distribution, and at intermediate energies for the α distribution), and a second one where the α -particle takes most of the energy (peaks at intermediate energies for the neutron and proton distributions and shoulder at high energies for the α -particle energy distribution).

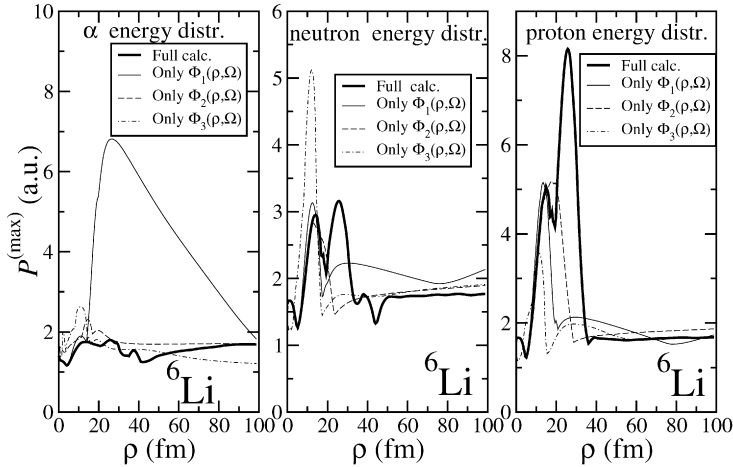


Fig. 13. Projections of kinetic energy distributions as functions of ρ for ${}^6\text{Li}$ (2^+). Thick curves: projection of the α (left panel) and proton (right panel) kinetic energy distributions (Fig. 10) on the $E_{\alpha,p}/E_{\alpha,p}^{(\max)} = 1$ plane. They are then the profile originated by the maximum values of the energy distribution for each value of ρ . The thin curves are the same profile but when only the first adiabatic term (solid), only the second adiabatic term (dashed), or only the third adiabatic term (dot-dashed) is included in the calculation.

In the lower part of the figure (α energy distribution) one can see that when ρ increases the α -particle emerges in a high-energy peak with a broad tail extending down to intermediate energies. While the high-energy peak reveals a decay through α -particle emission, the shoulder seen at intermediate and small energies can be a combination of direct decay and sequential decay through proton emission (the remaining α -neutron system populates the ${}^5\text{He}$ resonance). For large ρ the proton distribution resembles that of ${}^6\text{Be}$ with a peak moved a little towards the high-energy, while the neutron distribution exhibits a rather broad peak at low energy. This is again consistent with a contribution from sequential decay through proton emission, or equivalently through the ${}^5\text{He}$ resonance, but also with contributions from α -particle emission.

From Fig. 12 we observe that the neutron and proton kinetic energy distributions are again stable for large values of ρ , while for the α -particle energy distribution this stability is less clean. The details are shown in Fig. 13, where again we show the profile of the projection of the kinetic energy distributions on the $E_{\alpha,p}/E_{\alpha,p}^{(\max)} = 1$ plane. In the left panel we see how the profile of the α -particle kinetic energy distribution has a tendency to grow with ρ . In any case this tendency is not dramatic, and remarkably small if we compare to the behavior obtained including only the lowest adiabatic potential (solid thin curve) where we observe a strong decrease with ρ . Fortunately, the remaining adiabatic terms compensate to a great extent this behavior producing a total distribution we can consider acceptably stable.

The particular behavior of the α -particle kinetic energy distribution when only the first adiabatic potential is included can be understood from the left part of Fig. 4, where we see that in the first adiabatic potential, and the first Jacobi set (\mathbf{x} from neutron to proton) the clearly dominating component at large distances (solid thick curve) corresponds to $\ell_x = 0$. The existence of a very low lying virtual s -state in the neutron–proton interaction makes the contribution of this adiabatic term specially sensitive to α emission at high energy, while the two nucleons populate the virtual s -state.

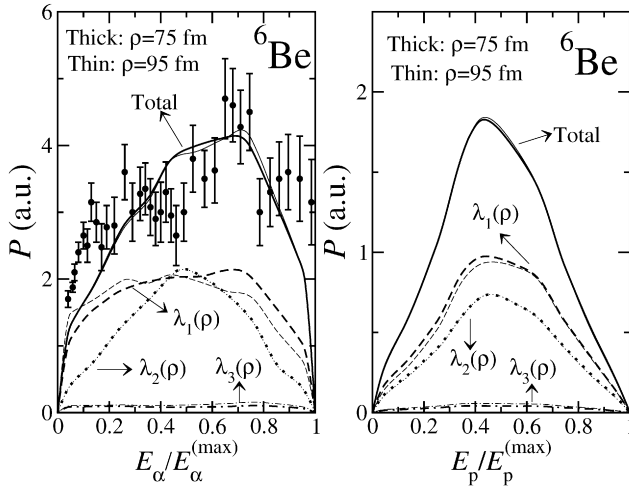


Fig. 14. The kinetic energy distribution of the α -particle (left) and the proton (right) after decay of the 2^+ -resonance in ${}^6\text{Be}$. The scaling angle is $\theta = 0.15$ and the two sets of curves are for $\rho = 75, 95$ fm. The points are from [7]. Contributions from the lowest adiabatic potentials are shown individually.

The three-dimensional plots of the kinetic energy distributions are not very useful in accurate descriptions. Furthermore, the numerical convergence and the microscopic origin of the different parts of the distributions cannot be seen in these plots. Therefore we show in Fig. 14 the distributions arising from angular wave functions for two different ρ -values for the ${}^6\text{Be}$ -decay. We first notice that the curves for the total distributions are almost identical demonstrating that the basis size is sufficiently large. The distributions are stable and the computed observables can meaningfully be compared with measurements. The α -particle distribution is within error bars in agreement with measurements. The total distributions are obtained by adding two fairly large contributions from the two lowest, and several smaller parts from the higher lying angular eigenfunctions, see also Fig. 6. The contribution from the lowest eigenfunction falls into two pieces for the α -particle, i.e. one peaked at low and one peaked at high energy. The second eigenfunction is more peaked in the middle at an intermediate energy. In total a broad distribution arises. For the protons the two contributions are both peaked at intermediate energies.

For the decay of ${}^6\text{Li}$ we show the corresponding results in Fig. 15. Again we observe that the total distributions are very similar for the two values of ρ . The two lowest angular eigenfunctions dominate the distributions. For the α -particle the first and second eigenfunctions peak at high and intermediate energies, respectively. For the neutron the peaks are at low and intermediate energies whereas the two proton contributions both peak at intermediate energies. The peaks of the proton and neutron distributions in Fig. 15 are moving in opposite directions compared to the ${}^6\text{Be}$ -decay in Fig. 14. The α -particle energy distribution is, at least qualitatively, in agreement with the measurements. Closer comparison is difficult since the experimental distribution only is available in the laboratory system.

6. Summary and conclusions

Three-body resonance decays with charged particles in the final state obviously on some level involve the three-body Coulomb problem in the continuum. We employ precisely the same nu-

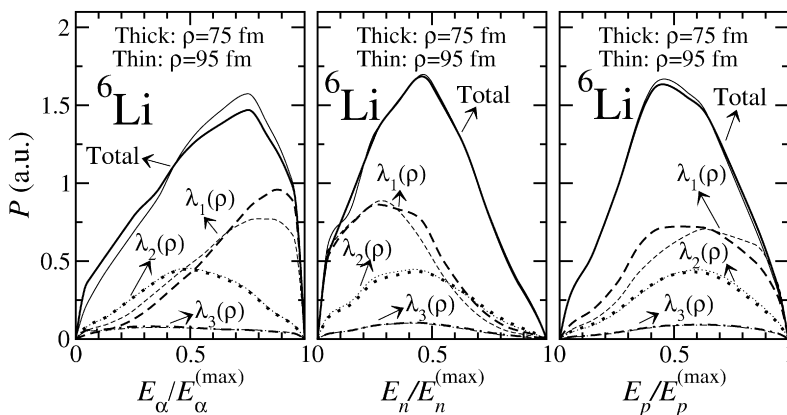


Fig. 15. The kinetic energy distribution of the α -particle (left), the neutron (middle) and the proton (right) after decay of the isobaric analogue 2^+ -resonance in ${}^6\text{Li}$. The scaling angle is $\theta = 0.10$ and the two sets of curves are for $\rho = 75, 95$ fm. Contributions from the lowest adiabatic potentials are shown individually.

merical method as used successfully for short-range interactions. We only add the Coulomb potentials. We choose the 2^+ -resonances in ${}^6\text{Be}$ and ${}^6\text{Li}$ as the specific examples. They are isobaric analogue states of a corresponding state ${}^6\text{He}$ where only short-range interactions are necessary. The discussions should be general and applicable as explanations for other similar systems.

We first calculate the adiabatic potentials and the hyper-angular wave functions by using hyperspherical coordinates and the complex scaling method. The asymptotic large-distance behavior of these potentials must be as the Coulomb potentials, i.e. ρ^{-1} where ρ is the hyperradius. However, the proportionality factor depends on the quantum numbers of the specific level as well as on the charges of the particles. We estimate these factors using the free wave functions with the proper angular momentum quantum numbers and without nodes in the remaining hyper-angle. The numerical results are consistent with the estimates, indicating convergence in the crucial region of intermediate distances.

The structures of the angular wave functions are seen in their partial wave expansion. We find strong variation of the non-diagonal coupling potentials up to distances of about 30 fm. This indicates that the large-distance asymptotic behavior is reached at these distances even in the presence of the Coulomb interaction. We investigate the dependence on ρ and find a strong variation of the individual components where a constant large-distance behavior not necessarily is reached although a smooth behavior in general essentially is established at 60–70 fm.

The radial wave functions are the ρ -dependent amplitudes on each of the angular eigenfunctions. Under resonance conditions the large-distance behavior must be oscillating, after complex scaling, and exponentially decreasing. The observable kinetic energy distributions are determined by the ratios of these individually vanishing radial wave functions. The precision of the numerical procedure is then delicate and must then be carefully checked. The kinetic energy distributions must be stable in an intermediate region of hyperradii, i.e. ρ must exceed the values where the rapid changes occur, but it should be small enough to allow a complete description in terms of the basis used. Such a region is found for each resonance decay between 60 and 90 fm.

For ${}^6\text{Be}$ only α -particle and protons emerge after the decay. Their distributions are consistent with components of different decay mechanisms, i.e. α -particle emission as the dominating part with significant contributions from both direct decay and sequential proton emission. The com-

putations are consistent with the measured distributions. For ${}^6\text{Li}$ the α -particle emission is even more dominating and proton emission also contributes substantially via the ${}^5\text{He}$ -resonance while neutron emission is much more suppressed compared to the decay of ${}^6\text{Be}$.

In conclusion, three-body decay of many-body resonance can be rather reliably computed by combining the adiabatic hyperspherical expansion and the complex scaling methods. The Coulomb interaction demands careful treatment of the convergence properties as functions of hyperradius and basis size. If the hyperradius is chosen too large the basis cannot describe the distributions, and if the hyperradius is chosen too small the asymptotic large-distance distribution is not reached.

References

- [1] E. Garrido, D.V. Fedorov, A.S. Jensen, H.O.U. Fynbo, Nucl. Phys. A 748 (2005) 27.
- [2] E. Garrido, D.V. Fedorov, A.S. Jensen, H.O.U. Fynbo, Nucl. Phys. A 748 (2005) 39.
- [3] E. Garrido, D.V. Fedorov, A.S. Jensen, H.O.U. Fynbo, Nucl. Phys. A 766 (2006) 74.
- [4] D.V. Fedorov, E. Garrido, A.S. Jensen, Few-Body Systems 33 (2003) 153.
- [5] K.P. Artemov, V.Z. Gol'berg, I.P. Petrov, V.P. Rudakov, I.N. Serikov, V.A. Timofeev, Yad. Fiz. 17 (1973) 225, Sov. J. Nucl. Phys. 17 (1973) 115.
- [6] O.V. Bochkarev, et al., JETP Lett. 40 (1984) 969;
O.V. Bochkarev, et al., JETP Lett. 42 (1985) 374;
O.V. Bochkarev, et al., JETP Lett. 42 (1985) 377.
- [7] B.V. Danilin, M.V. Zhukov, A.A. Korshennikov, L.V. Chulkov, V.D. Efros, Sov. J. Nucl. Phys. 46 (1987) 225.
- [8] O.V. Bochkarev, et al., Nucl. Phys. A 505 (1989) 215.
- [9] O.V. Bochkarev, A.A. Korshennikov, E.A. Kuz'min, I.G. Mukha, L.V. Chulkov, G.B. Yan'kov, Yad. Fiz. 55 (1992) 1729, Sov. J. Nucl. Phys. 55 (1992) 955.
- [10] R.J. Kryger, et al., Phys. Rev. Lett. 74 (1995) 860.
- [11] C.R. Bain, et al., Phys. Lett. B 373 (1996) 35.
- [12] G. del Campo, et al., Phys. Rev. Lett. 86 (2001) 43.
- [13] J. Giovinazzo, et al., Phys. Rev. Lett. 89 (2002) 102501.
- [14] M. Pfützner, et al., Eur. Phys. J. A 14 (2002) 279.
- [15] M.J. Chromik, et al., Phys. Rev. C 66 (2002) 24313.
- [16] H.O.U. Fynbo, et al., Phys. Rev. Lett. 91 (2003) 82502.
- [17] B. Blank, J. Giovinazzo, M. Pfützner, C. R. Physique 4 (2003).
- [18] T. Zerguerras, et al., Eur. Phys. J. A 20 (2004) 389.
- [19] B. Blank, et al., Phys. Rev. Lett. 94 (2005) 232501.
- [20] E. Nielsen, D.V. Fedorov, A.S. Jensen, E. Garrido, Phys. Rep. 347 (2001) 373.
- [21] D.V. Fedorov, A.S. Jensen, H.O.U. Fynbo, Nucl. Phys. A 718 (2003) 685c.
- [22] E. Garrido, D.V. Fedorov, A.S. Jensen, Eur. Phys. J. A 25 (2005) 365.
- [23] A. Csoto, Phys. Rev. C 49 (1994) 3035.
- [24] N. Tanaka, Y. Suzuki, K. Varga, Phys. Rev. C 56 (1997) 562.
- [25] V. Vasilevsky, A.V. Nesterov, F. Arickx, J. Broeckhove, Phys. Rev. C 63 (2001) 034607.
- [26] F.C. Barker, Phys. Rev. C 68 (2003) 054602.
- [27] P. Descouvemont, E. Tursunov, D. Baye, Nucl. Phys. A 765 (2006) 370.
- [28] L.V. Grigorenko, M.V. Zhukov, Phys. Rev. C 68 (2003) 054005.
- [29] D.V. Fedorov, A.S. Jensen, Phys. Lett. B 389 (1996) 631.
- [30] T.N. Rescigno, M. Baertschy, W.A. Isaacs, C.W. McCurdy, Science 286 (1999) 2474.
- [31] A. Cobis, D.V. Fedorov, A.S. Jensen, Phys. Rev. C 58 (1998) 1403.
- [32] A. Cobis, A.S. Jensen, D.V. Fedorov, J. Phys. G 23 (1997) 401.
- [33] D.R. Tilley, C.M. Cheves, J.L. Godwin, G.M. Hale, H.M. Hofmann, J.H. Kelley, C. G. Sheu, H.R. Weller, Nucl. Phys. A 708 (2002) 3.
- [34] D.V. Fedorov, A.S. Jensen, K. Riisager, Phys. Rev. C 49 (1994) 201.